Materials Advances

ROYAL SOCIETY OF CHEMISTRY

PAPER

View Article Online
View Journal | View Issue

Cite this: *Mater. Adv.*, 2025, 6, 6575

Substrate-induced strain control of (Mn, Fe, Co, Ni)-doping effects in $SrTiO_3$ thin films

M. Tyunina, *[ab] N. Nepomniashchaia, [b] O. Pacherova,[b] T. Kocourek,[b] V. Vetokhina[b] and A. Dejneka[b]

Received 9th July 2025,
Accepted 13th August 2025

DOI: 10.1039/d5ma00732a

rsc.li/materials-advances

Tailoring chemical composition is the primary route to achieving desired properties of materials, including technologically important ABO_3-type perovskite oxides. This approach is generally assumed to translate directly to thin films. In contrast, this study demonstrates that substrates can significantly modify compositional effects in thin films. Specifically, transition-metal (M = Mn, Fe, Co, Ni) substitution is experimentally investigated in thin films of the archetypal perovskite $SrTiO_3$ grown by pulsed laser deposition on different substrates. It is found that substrate-induced lattice strain regulates the preferential sites for M substitution and leads to an increase in the direct optical bandgap. In the absence of strain, doping with M cations has no effect on the bandgaps. Substrate-imposed strain and/or substitution are found to induce band tailing and weak sub-gap optical absorption. These findings highlight the unique role of substrates in engineering the chemical composition and functional properties of thin films.

Introduction

Strontium titanate ($SrTiO_3$, or STO) is an archetypal representative of ABO_3-type perovskite-structure metal oxides. As one of the most extensively studied perovskites, STO serves as an excellent platform for exploring the fundamentals of this scientifically fascinating and technologically important class of ABO_3 oxides. STO belongs to a family of ABO_3-type wide-bandgap insulators and ferroelectrics, which exhibit various polarization states (*i.e.*, paraelectric, ferroelectric, antiferroelectric, and relaxor) and possess outstanding properties such as large dielectric permittivity and strong piezoelectric, electrooptic, pyroelectric, and electrocaloric effects.[1–3] These properties enable a wide range of mainstream electronic and photonic devices—from commercialized technologies to highly innovative applications—including modern energy storage, harvesting, and conversion, as well as memory and computing.[2–9]

Beyond mainstream developments, substantial effort has been devoted to applications in photocatalysis and photovoltaics,[10–12] where STO-based photocatalysis is well established.[13–25] In these contexts, the photogeneration, separation, and transport of charge carriers are critical, with solar-reliant applications requiring visible-light absorption. However, these desired properties conflict with the fundamental electronic band structure, which features wide bandgaps above 3 eV and excellent insulating behavior. Since ABO_3 perovskites can accommodate a broad variety of cationic substitutions without losing phase stability, the primary strategy to overcome this conflict is through appropriate cationic doping. For STO, this approach has proven viable with transition metals (denoted M) such as Mn,[26–32] Fe,[33–42] Co,[43–50] and Ni.[51–54]

M cations can exhibit multiple valence states ($M^{2+}/M^{3+}/M^{4+}$) and, in principle, substitute at both the Ti site (denoted M(Ti)) and the Sr site (denoted M(Sr)) in STO (see SI, Table S1).[55] Dual-site occupancy—M(Ti) and M(Sr)—has been reported for Mn,[26–30] Fe,[38–42] and Co,[49,50] whereas only Ti-site substitution has been observed for Ni.[52–54] First-principles theoretical calculations indicate a general tendency for M substitutions to create local lattice distortions and multiple in-gap states (*i.e.*, occupied or unoccupied energy levels within the bandgap).[30–32,39–42,49,50,52–54] It has been found that local bond contraction and lattice distortion typically occur around M(Ti) substitutions, whereas M(Sr) substitutions tend to be strongly off-centered and induce significant lattice expansion. While these M-induced local deformations are generally unimportant for phase stability and properties in MSTO ceramics, powders, and particles, they can play a crucial role in thin films, as demonstrated in this work.

Thin films now constitute an essential and integral field of modern materials research. While tailoring a material's chemical composition remains the primary route to achieving desired properties, thin films offer unique pathways through substrate-controlled phenomena. Notably, for a given chemical

[a] *Microelectronics Research Unit, Faculty of Information Technology and Electrical Engineering, University of Oulu, P. O. Box 4500, FI-90014 Oulu, Finland. E-mail: marina.tjunina@oulu.fi*
[b] *Institute of Physics of the Czech Academy of Sciences, Na Slovance 2, 18221 Prague, Czech Republic*

composition, the film's crystal structure, morphology, lattice strain, and many functional responses can be significantly altered by varying the substrate.

In various ABO_3 perovskite films—including single-crystal-type epitaxial films[56]—the effects of substrate-induced strain have been extensively studied since the seminal works on STO and other titanates.[57–61] Lattice strain originates from a mismatch between the film and substrate lattice parameters in epitaxial films (referred to as "misfit strain") and from differences in thermal expansion coefficients in all films grown at high temperatures (referred to as "thermal strain"). In STO, substrate-imposed strain has been shown to induce ferroelectric phases, widen the bandgap, and alter dielectric permittivity.[58,59,62,63]

In contrast, the impact of substrates is often overlooked when considering the effects of chemical doping. It is generally assumed that M substitution should occur and influence properties in thin M-doped STO (MSTO) films in the same way as in MSTO ceramics or crystals. Contrary to this expectation, we demonstrate here a significant influence of substrates on M-site occupancy and the band structure in thin MSTO films.

In this work, the crystal structure and optical absorption are experimentally investigated in thin films of pure STO and M-doped STO (M = Mn, Fe, Co, or Ni) grown on diverse substrates to induce varying degrees of substrate-imposed strain. It is revealed that in thin films, the preferential substitution sites (Ti or Sr) for M cations are constrained by the substrate. These constraints are suggested to originate from elastic coupling between local deformations induced by substitutions and global deformations imposed by the substrate. Furthermore, it is shown that doping STO with up to a few percent of M cations has no effect on the direct bandgap or fundamental optical absorption. In contrast, substrate-imposed strain leads to an increase in the direct bandgap and suppression of the indirect bandgap. Substrate strain and/or doping are also found to produce band tailing and only weak sub-gap absorption. These findings strongly imply that, compared to bulk materials, the presence of a substrate can dramatically alter the expected doping effects in thin films.

Methods

Thin (~150 nm) films of pure STO and M-doped STO (MSTO with M = 2 at% of Mn, Fe, Co, or Ni) were prepared by pulsed laser deposition (PLD) at elevated temperature and high pressure of ambient oxygen.[63–66] Compared to other vapor deposition techniques such as, for instance, molecular beam epitaxy, PLD allows for high pressure of oxygen gas ambience during deposition. This capability is critical for maintaining and tuning the oxygen stoichiometry of oxide thin films, thereby enabling the synthesis of a broad spectrum of complex metal oxides, including perovskite oxides.[56] The key deposition parameters were as follows: wavelength of laser radiation 248 nm, laser fluence 2 J cm^{-2}, substrate temperature 700 °C, and oxygen pressure 20 Pa. To ensure growth of epitaxial strained films, single-crystal (001)-oriented $(LaAlO_3)_{0.3}(Sr_2AlTaO_6)_{0.7}$ (LSAT) substrates were used. For strain-free epitaxial films, the (001) STO substrates were employed. To vary thermal strain, substrates of Si and SiO_2 (fused silica) were utilized. The proper elemental composition of the films was verified as before.[66] Room-temperature crystal structure of the films was inspected by X-ray diffraction (XRD) using Cu Kα radiation on a SmartLab SE Multipurpose diffractometer (Rigaku Corp.), a D8 DISCOVER diffractometer (Bruker Corp.), and an Empyrean diffractometer (Malvern Panalytical). Also X-ray reflectivity (XRR) was measured on the D8 DISCOVER diffractometer. The optical properties of the films and substrates were studied using variable angle spectroscopic ellipsometry. The measurements were performed on a J. A. Woollam VUV VASE ellipsometer at room temperature. The optical dielectric functions were extracted from the spectra of ellipsometric angles using a commercial WVASE32 software package. The optical absorption coefficient was calculated from these dielectric functions. More details on the ellipsometry measurements and data processing can be found elsewhere.[63,65,67]

Results and discussion

Elastic control of substitution sites

Perovskite structure films of STO and MSTO of similar thicknesses are obtained on different substrates (Fig. 1, 2 and Fig. S1–S4, SI).

The films on LSAT are epitaxial, (001)-oriented, with the (00*l*) planes and [100] and [010] directions parallel to those of the substrates (Fig. 1a and 2 and Fig. S1, S2, SI). This cube-on-cube-type epitaxial growth of STO on LSAT is well-known.[59,68] Because of the film-substrate mismatch in the lattice parameters, there is

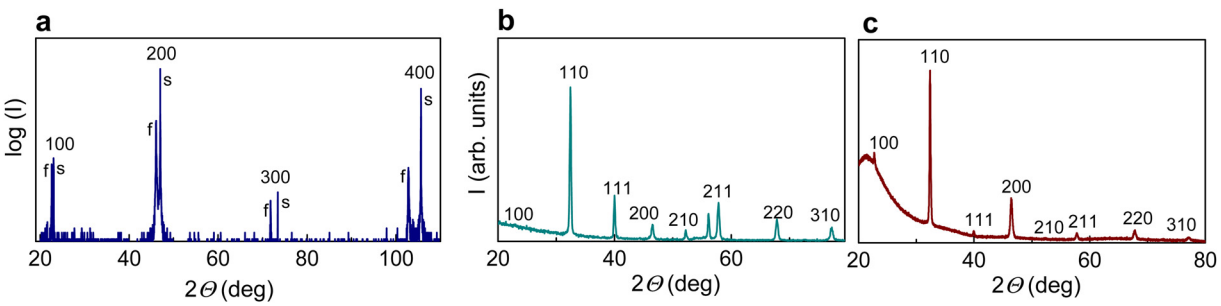

Fig. 1 XRD ω-2Θ scans in the MSTO films on (a) LSAT, (b) Si, and (c) SiO_2 substrates. All perovskite peaks are indexed. In (a), the peaks from the films and substrates are marked by "f" and "s", correspondingly.

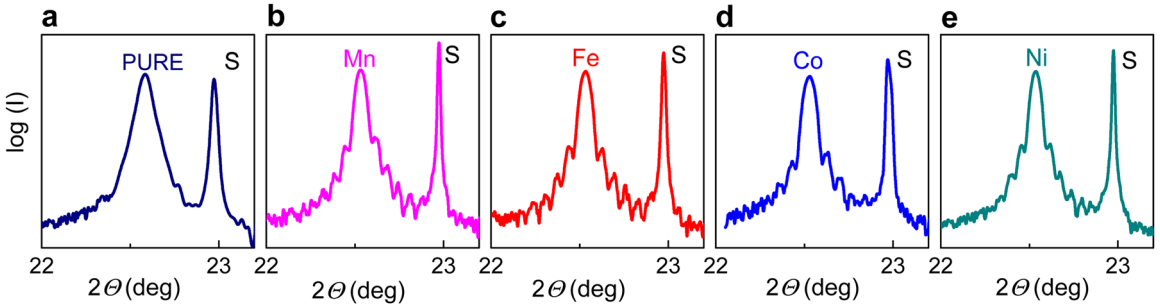

Fig. 2 Details of the ω-2Θ XRD scans around the (001) perovskite peaks in (a) STO and (b)–(e) MSTO on LSAT. The peaks from substrates are marked by "s". The M-substitutions are marked on the plots in (b)–(e).

a misfit strain in the STO/LSAT and MSTO/LSAT films (SI, SI2, expressions S1–S6). The theoretical room-temperature in-plane misfit strain is compressive $s_a \approx -1\%$ leading to an elongated out-of-plane lattice parameter in the films. The out-of-plane parameters measured in the films are larger than 3.905 Å in crystal, that qualitatively agrees with the substrate-induced in-plane compression.

The films on Si and SiO_2 substrates are polycrystalline (Fig. 1b, c and Fig. S3, S4, SI). The films are grown at high temperature so that the film-substrate mismatch in thermal expansion coefficients leads to a thermal strain, which builds up during cooling (SI, SI3) and is in-plane tensile here. (The thermal strain is negligible in the films on LSAT). The room-temperature strain is very weak (not detected) in the films on Si, and it is approximately 0.3% in the films on SiO_2.

The doped MSTO/LSAT films are of excellent epitaxial quality. The XRD Laue oscillations are well-expressed around the (001) and (002) perovskite peaks therein (Fig. 2b–e and Fig. S1g–j). The films are fully in-plane aligned with the underlying substrates (Fig. S2b). These observations contrast with the expected partial relaxation of misfit strain with increasing thickness.[65,68] The critical thickness, at which the relaxation of misfit strain begins, is approximately 60–80 nm in STO/LSAT.[65,68] Here, the partial relaxation is evidenced in the 150-nm-thick pure STO/LSAT film (Fig. 2a and Fig. S1f and S2a), but not in the 150-nm-thick MSTO/LSAT films. Furthermore, compared to the theoretical out-of-plane lattice parameters $c \approx 3.927$ Å in STO/LSAT, the parameters are large, $c \approx 3.942$ Å, in the MSTO/LSAT films. Although contraction of MSTO compared to STO might explain a smaller misfit and a larger critical thickness, it also suggests a smaller parameter c in the MSTO/LSAT films, which is against the observations. The concurrent rise of the critical thickness and of the out-of-plane strain indicates a peculiar effect of doping in epitaxial films.

Next, this effect is considered in terms of local deformations associated with M-substitutions in STO.[30–32,39–42,49,50,52–54] Compared to atomic positions in perovskite-structure STO (Fig. 3a), the atoms are displaced, and different types of local lattice distortions arise around M-substitutions for Ti, M(Ti) and M-substitutions for Sr, M(Sr), in MSTO. In pure STO, Ti is surrounded by 6 oxygen atoms in the TiO_6 octahedra (Fig. 3a). When Ti is substituted with M (Fig. 3b), the MO_6 entity

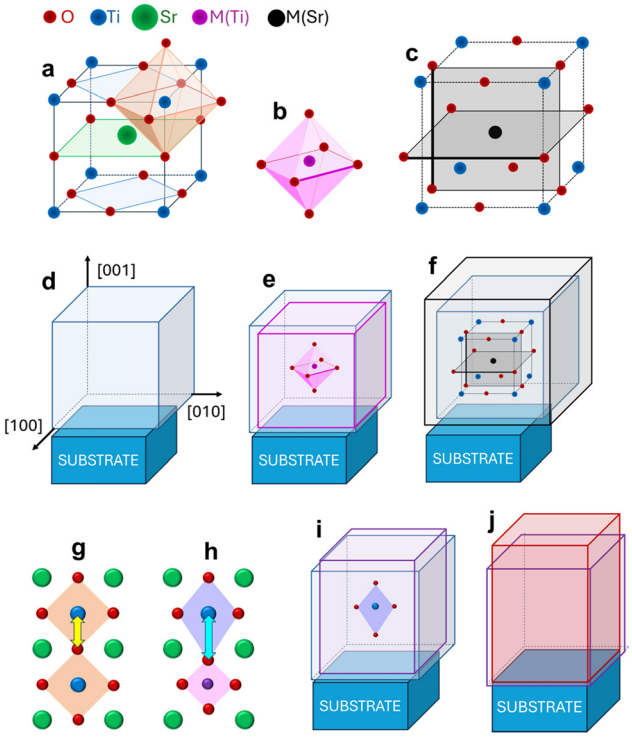

Fig. 3 Schematics of ((a)–(c), (g) and (h)) atomic positions and ((d)–(f), (i) and (j)) unit cells of ((a), (d) and (g)) STO and ((b), (c), (e), (f), (i) and (j)) MSTO for ((b), (e), (h)–(j)) M(Ti) and ((c) and (f)) M(Sr) substitutions.

experiences a uniform contraction, so that both the M–O and O–O distances diminish. Lattice distortions associated with M-substitution for Sr, M(Sr), are more complex. In pure STO, the local structure around Sr can be thought of as a cube with the Ti atoms in its corners and Sr in its center (Fig. 3a). The distances between the apical oxygen atoms located in the TiO_2 planes (*i.e.*, the O–O distances along the vertical sides of the cube in Fig. 3a) and between the equatorial oxygen atoms in the SrO-plane (along the horizontal direction in Fig. 3a) are similar. The M(Sr) substitutions produce severe deformation: the lattice around M(Sr) is not cubic anymore and, compared to the central position of Sr in STO, the M(Sr) is off-centered. The MO planes experience massive expansion compared to the SrO ones. For instance, elongations of the O–O distances can reach nearly 10% for M = Mn.[31]

In epitaxial (001)-oriented films grown on LSAT, the lattice is biaxially compressed in-plane and contracts accordingly (Fig. 3d). The possible contraction of the MO_6 octahedra due to M(Ti) substitutions aligns with the substrate-induced contraction. Therefore, the placement of M substitutions at the Ti sites is elastically favoured in MSTO/LSAT films (Fig. 3e). Conversely, the possible expansion associated with M(Sr) substitutions opposes the substrate-induced contraction. As a result, the placement of M substitutions at the Sr sites is elastically unfavourable in MSTO/LSAT films (Fig. 3f). During the high-temperature growth of thin films, atoms migrate across the film's surface. This surface migration enables M atoms to reach and occupy elastically favorable Ti sites. In this way, the substrate-induced compressive strain promotes M substitution at Ti sites (Fig. 3e) and suppresses M substitution at Sr sites (Fig. 3f).

Compared to STO, the lattice parameters of MSTO should decrease for the M(Ti) substitutions. Experimentally, the lattice parameters of unstressed MSTO (*i.e.*, of MSTO material, which is a free-standing prototype of the film) can be extracted from the measured lattice parameters of the films (SI, SI3). The extracted lattice parameter of cubic unstressed MSTO (SI, SI3, expressions S3–S6) is large $\sim$3.914 Å that contradicts the observed excellent epitaxy. Such parameter suggests $\sim$1.2% film-substrate misfit leading to a smaller critical thickness and worse epitaxial quality of the doped films compared to pure ones, which is not the case. Therefore, unstressed MSTO is assumed to be metrically tetragonal instead of cubic (Fig. 3i),[69] with the lattice parameters $a_t = b_t < c_t$ extracted correspondingly (SI, SI3, expressions S7–S12). The small found parameter a_t = 3.894 Å implies misfit being reduced to $\sim$0.7%, that complies with the observed excellent MSTO/LSAT epitaxy.

The unveiled tetragonality of unstressed MSTO can be related to macroscopic elastic interactions, not captured by atomic-scale first-principles calculations.[69] It is known that deformations around point defects lead to elastic dipole tensors, or elastic dipoles.[70,71] Generally, elastic dipoles are randomly oriented. However, anisotropic dipoles align along a certain crystallographic direction in epitaxial films.[69] Here, anisotropic elastic dipoles might be caused by deformations in vicinity of the M(Ti) substitutions. Compared to the same Ti–O distances everywhere in STO (Fig. 3g), the distance between Ti and apical O atom, which belongs to the contracted MO_6 octahedron (or the Ti–O_M distance for brevity) is enlarged (Fig. 3h). The Ti–O_M elongation suggests the presence and alignment of anisotropic elastic dipoles, such that the Ti–O_M bonds are oriented along the out-of-plane direction in the MSTO/LSAT films (Fig. 3i). For the prototype unstressed MSTO material of the films, the Ti–O_M alignment leads to tetragonality. For the MSTO films stressed by LSAT substrates, the alignment reduces the total elastic energy, raises the critical thickness, and enhances the out-of-plane strain. More details on this mechanism can be found in ref. 69.

Thus, our observations indicate that the Ti sites for M-substitutions are elastically preferable in epitaxial MSTO films subjected to the substrate-induced in-plane compression. Notably, elastic considerations for substrate controlled substitutional sites are applicable to epitaxial films of other materials on diverse substrates in general.

Clearly, using different substrates allows for regulating lattice strains and for promoting selected substitutional sites. Here, the STO and MSTO films are grown on different substrates and, hence, possess different in-plane strains: compressive on LSAT, zero on STO, weak near-zero tensile on Si, and tensile on SiO_2. The films contain no substitutions (in STO), preferably M(Ti) substitutions (in MSTO on LSAT), or allow for both M(Ti) and M(Sr) substitutions (in MSTO on STO, Si, and SiO_2). The prepared variety of films makes it possible to distinguish the roles of strains and/or dopants in the electronic energy band structure as shown next.

Optical absorption and band structure

To experimentally assess the main characteristics of the electronic energy band structure, including bandgaps and in-gap states, the optical absorption spectra were investigated in the STO and MSTO films and in the reference (001)-oriented STO crystal.

In the STO crystal, fundamental optical absorption sets at the photon energy of $\sim$4 eV, and the absorption spectrum contains two dominant peaks at $\sim$5 eV and $\sim$6.5 eV (Fig. 4a). These features are determined by the direct optical transitions from the valence band (VB) to the conduction band (CB). The lowest-energy direct interband transition is associated with the direct bandgap, whose energy E_D = 3.86 eV is found from the Tauc plot for direct gap[72–77] (Fig. 4b). Details of direct transitions are

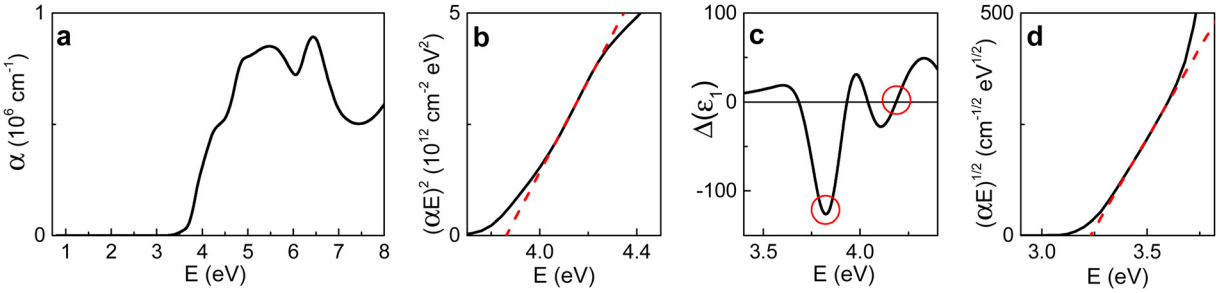

Fig. 4 Optical absorption in the unstressed (001)STO crystal: (a) absorption coefficient as a function of photon energy; (b) Tauc plot for direct gap; (c) second derivative of the real part of the dielectric function, $\Delta(\varepsilon_1)$; (d) Tauc plot for indirect gap. Dashed lines show fit in ((b) and (d)). Circles mark the energies of the critical points (CPs) in (d).

usually obtained from the critical point (CP) analysis using the second derivative of the dielectric function.[78–80] In the reference crystal, the lowest energy CP involves the main CP1-line at E_{CP1} = 3.82 eV and the weaker CP2-line at E_{CP2} = 4.19 eV (Fig. 4c). The detected energies E_D and E_{CP1} are very close to each other, confirming the direct bandgap of ~3.8 eV. We note that the direct interband transitions determine strong absorption: the absorption coefficient is $\alpha \sim 10^6$ cm^{-1} for $E > 3.7$ eV (Fig. 4a). A weaker near-edge absorption ($\alpha \sim 10^4$ cm^{-1}) is related to an indirect interband transition, with the indirect bandgap energy E_I = 3.23 eV found from the Tauc plot for indirect gap (Fig. 4d). The results in Fig. 4 are consistent with the well-known band structure of STO, testify to the high accuracy of our analysis, and serve for comparison in the films investigations.

At first glance, in all films, the optical absorption spectra closely resemble that in the crystal (SI, Fig. S6). However, further analysis revealed differences.

Compared to the STO crystal, the strained STO/LSAT and MSTO/LSAT films exhibit a spectral shift to higher energy, or blueshift in the direct bandgaps (Fig. 5a, e and SI, Fig. S7) and in the critical points (Fig. 5b, f, SI, Fig. S8). Interestingly, the CP2-line is suppressed, in agreement with the previous observations in fully strained STO/LSAT.[63] Contrary to the obvious indirect gap in the crystal (Fig. 4d), there is no clear evidence for the indirect gap in the films on LSAT (Fig. 5c, g, SI, Fig. S9). Again, the strain-induced frustration of the indirect transition was found in STO before.[63] In the films on LSAT, instead of the clear indirect interband transition, the absorption edge ($E < 3.7$ eV) is Urbach-type [$\alpha \propto \exp(E/E_U)$][81–89] as evidenced by the linear plots [$\log(a) \propto E$] (Fig. 5d and h). The Urbach-type absorption suggests the presence of tails of the conduction and/or valence bands, with the tails' in-gap depth being described by the Urbach energy E_U. In the STO/LSAT film, the accessed energy $E_U \approx 0.14$ eV is large compared to that for a thermal band tailing and, accordingly, points to structural, strain-induced tailing.[81,89] In the MSTO/LSAT films, the energy E_U increases gradually with Ni, Co, Fe, Mn doping (Fig. 5h), that indicates also M-contributions to tailing. The energy levels of the Mn(Ti)-induced states are likely to be very close to the band edges (*e.g.*, to the bottom of the conduction band) and, accordingly, the Mn(Ti) states efficiently participate in tailing. On the other hand, the Ni(Ti) states may not contribute to tailing because of their deeper in-gap energy levels.

Table 1 summarizes the strain- and dopant-dependent characteristics of the optical absorption in the STO and MSTO films on LSAT. The energies are determined with the accuracy of ±0.02 eV. Nevertheless, the main effects are clear. The presence of strain leads to an increase in the direct bandgap, frustration of the indirect bandgap, and band tailing. The presence of M(Ti) substitutions has no effect on the bandgaps but enhances the band tailing. The energy separation between the band edge and the M-induced states is likely the smallest for M = Mn and gradually increases for M = Fe, Co, and Ni, correspondingly.

The results in Fig. 5 and Table 1 show the dominant influence of the substrate-induced strain on the electronic energy band structure of STO, whereas the substrate-controlled M(Ti) substitutions provide only minor contributions to the band tailing.

To better identify effects of the M(Ti) and M(Sr) substitutions on the band structure, the optical absorption spectra were

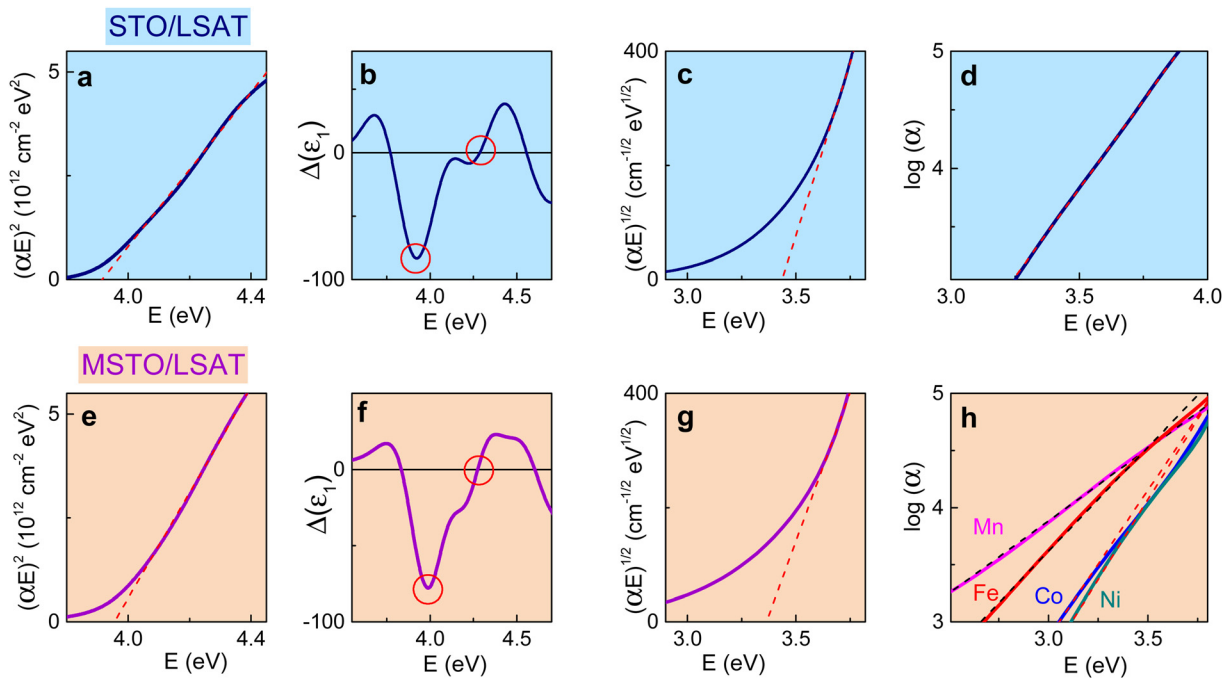

Fig. 5 Optical absorption in epitaxial films of ((a)–(d)) STO and ((e) and (f)) MSTO on LSAT: ((a) and (e)) Tauc plot for direct gap; ((b) and (f)) second derivative of the real part of the dielectric function, $\Delta(\varepsilon_1)$; ((c) and (g)) Tauc plot for indirect gap; ((d) and (h)) semi-log plots of the absorption coefficient as a function of photon energy. Dashed lines show fits in ((a), (d), (e) and (h)). Circles mark the energies of the critical points (CPs) in ((b) and (f)).

Table 1 The characteristic energies extracted from the optical absorption spectra in the STO/LSAT and MSTO/LSAT films

	Dopant M	Strain s_c, %	Direct gap E_D, eV	Critical point E_{CP1}, eV	Critical point E_{CP2}, eV	Indirect gap E_I, eV	Urbach tail E_U, eV
STO (crystal)	—	0	3.86	3.82	4.19	3.23	—
STO/LSAT	—	0.7	3.91	3.93	4.30	3.4[a]	0.14
MSTO/LSAT	Mn	1.0	3.96	4.00	4.25	[b]	0.34
	Fe	1.0	3.96	4.03	4.30	[b]	0.24
	Co	1.0	3.95	4.01	4.32	[b]	0.17
	Ni	1.0	3.95	3.96	4.28	[b]	0.16

[a] The gap is frustrated. [b] The indirect gap is frustrated and cannot be detected.

analyzed in the stress-free films on STO, weakly expanded films on Si, and expanded films on SiO_2 taking M = Mn as a representative case (Fig. 6 and Table 2). There are no detectable effects of doping on the direct bandgap (Fig. 6a, b, e, f, i and j). The formal Tauc fits for indirect gap are questionable in all films, making it impossible to accurately assess the indirect bandgap (Fig. 6c, g and k). However, the Mn-induced increase of sub-gap absorption, or redshift of the absorption edge to lower energies, is obvious (Fig. 6c, g and k). Interestingly, the formal Urbach fit shows a nonsensical two-component tailing in the MSTO films on STO and Si (Fig. 6d and h). This observation indicates an additional optical transition at ~3.2 eV suggesting an in-gap Mn-induced state, most probably – an occupied state close to the top of the valence band. This

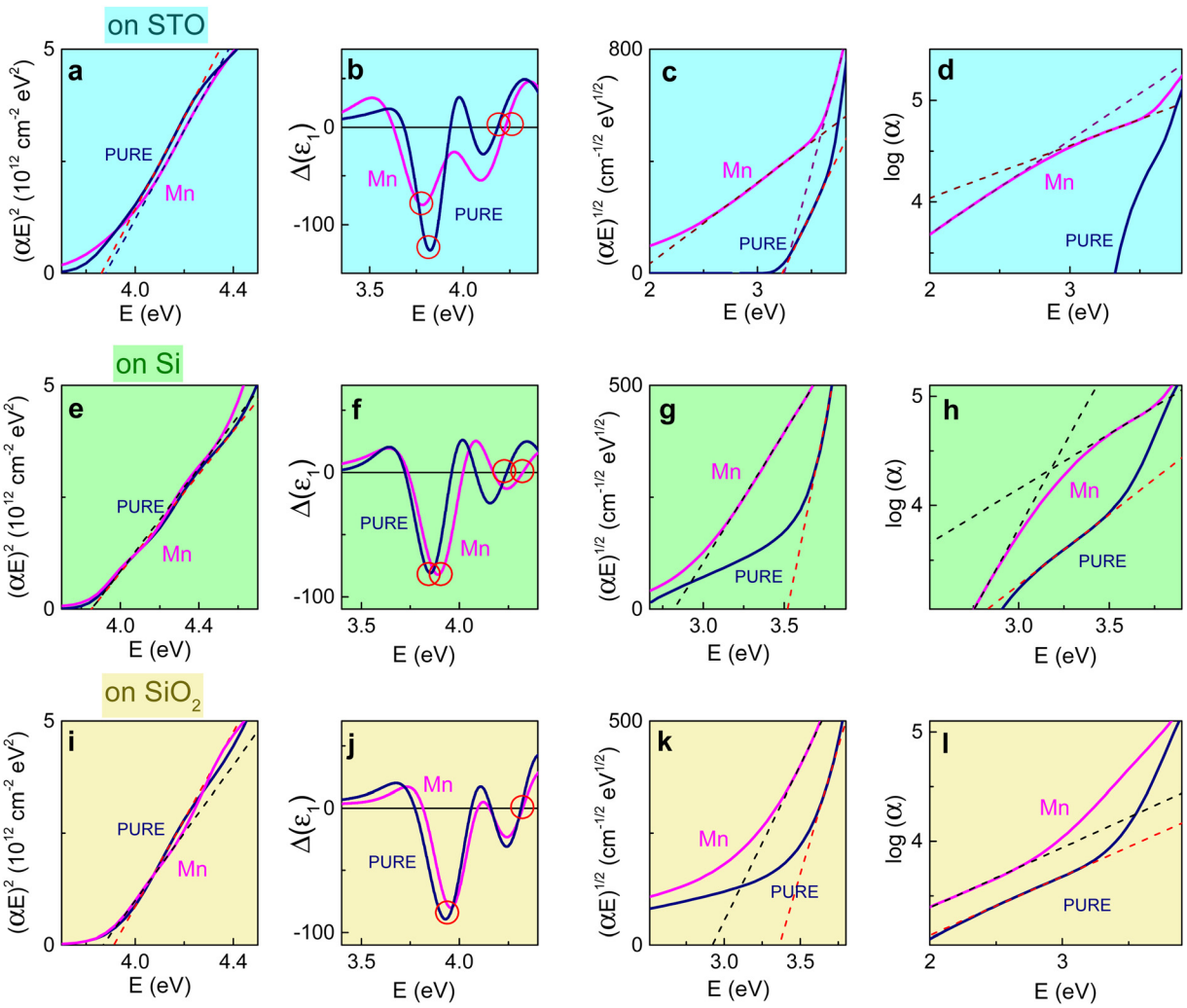

Fig. 6 Optical absorption in thin films of STO and MSTO on ((a)–(d)) STO, ((e) and (h)) Si, and ((i)–(l)) SiO_2 substrates: ((a), (e) and (i)) Tauc plot for direct gap; ((b), (f) and (j)) second derivative of the real part of the dielectric function, $\Delta(\varepsilon_1)$; ((c), (g) and (k)) Tauc plot for indirect gap; ((d), (h) and (l)) semi-log plots of the absorption coefficient as a function of photon energy. Dashed lines show fits in ((a), (d), (e), (h), (l) and (l)). Circles mark the energies of the critical points (CPs) in ((b) and (f)).

Table 2 The characteristic energies extracted from the optical absorption spectra in the STO and Mn–STO films on STO, Si, and SiO_2 substrates

	s_t, %		E_D, eV	E_{CP1}, eV	E_{CP2}, eV	E_I, eV	E_U, eV
STO	0	—	3.86	3.82	4.19	3.23	—
STO	0	Mn	3.87	3.78	4.23	3.25	0.83/0.47
Si	>0	—	3.85	3.85	4.25	3.5[a]	0.33
Si	>0	Mn	3.85	3.88	4.32	2.8[a]	0.14/0.43
SiO_2	0.3	—	3.87	3.92	4.30	3.2[a]	0.81
SiO_2	0.3	Mn	3.89	3.95	4.30	2.9[a]	0.79

[a] The gap is frustrated.

transition overlaps with band tailing in the film on SiO_2 (Fig. 6l). Notably, in contrast to the pronounced Mn-induced sub-gap absorption, doping with Ni produces much weaker changes (SI, Fig. S10).

The results in Fig. 6, Fig. S12 and Table 2 imply that M-substitution has no effect on the energies of the direct and indirect bandgaps but can rather lead to band tailing and sub-gap absorption in stress-free films. We note that, similarly, M-substitution has no effect on the bandgaps but enhances band tailing in strained films (Fig. 5 and Table 1).

The experimentally detected M-induced band tailing and sub-gap absorption can be ascribed to M-related in-gap states close to the top of the valence band and/or bottom of the conduction band. The M(Ti) substitutions may produce unoccupied states (empty energy levels) at the bottom of the conduction band or close to it inside the gap, whereas the M(Sr) substitutions – occupied states at the top of the valence band or close to it inside the gap. It is likely that the energy separation between the in-gap states and band edges is dopant-specific, namely: within the sequence of M = Mn, Fe, Co, Ni, the separation increases for the unoccupied M(Ti) states and decreases for the occupied M(Sr) states. Indeed, the detected optical band tailing is better expressed for Mn than for Ni in MSTO (Fig. 5h), and the absorption hump is observed for M = Mn (Fig. 6d and h) but not for M = Ni (SI, Fig. S10).

The observed optical absorption may be interpreted as follows (Fig. 7a–d). Compared to STO (Fig. 7a), the direct bandgap is not changed in MSTO (Fig. 7c). The M(Ti)-caused empty states at the bottom of the conduction band lead to the band's tailing and partial frustration of the indirect interband transitions in MSTO (Fig. 7c) compared to the clear indirect gap and transitions in STO (Fig. 7a). The M(Sr)-caused occupied states at the top of the valence band enable additional optical transitions (Fig. 7c) and, correspondingly, a weak hump in absorption (Fig. 7d), which can overlap with the tail. Importantly, there is no influence of doping on the direct bandgap and fundamental absorption ($\alpha \sim 10^6$ cm^{-1}). Only orders-of-magnitude weaker absorption tails ($\alpha \sim 10^3$–10^4 cm^{-1}) can spread to photon energies smaller than the direct gap.

Compared to unstressed STO and MSTO (Fig. 7a–d), the presence of substrate-imposed strain leads to a significant increase in the direct bandgap, frustration of the indirect transitions, and band tailing (Fig. 7e and f). The strain-caused band tailing can be enhanced by M-doping (Fig. 7g). Again, there is no influence of doping on the direct bandgap

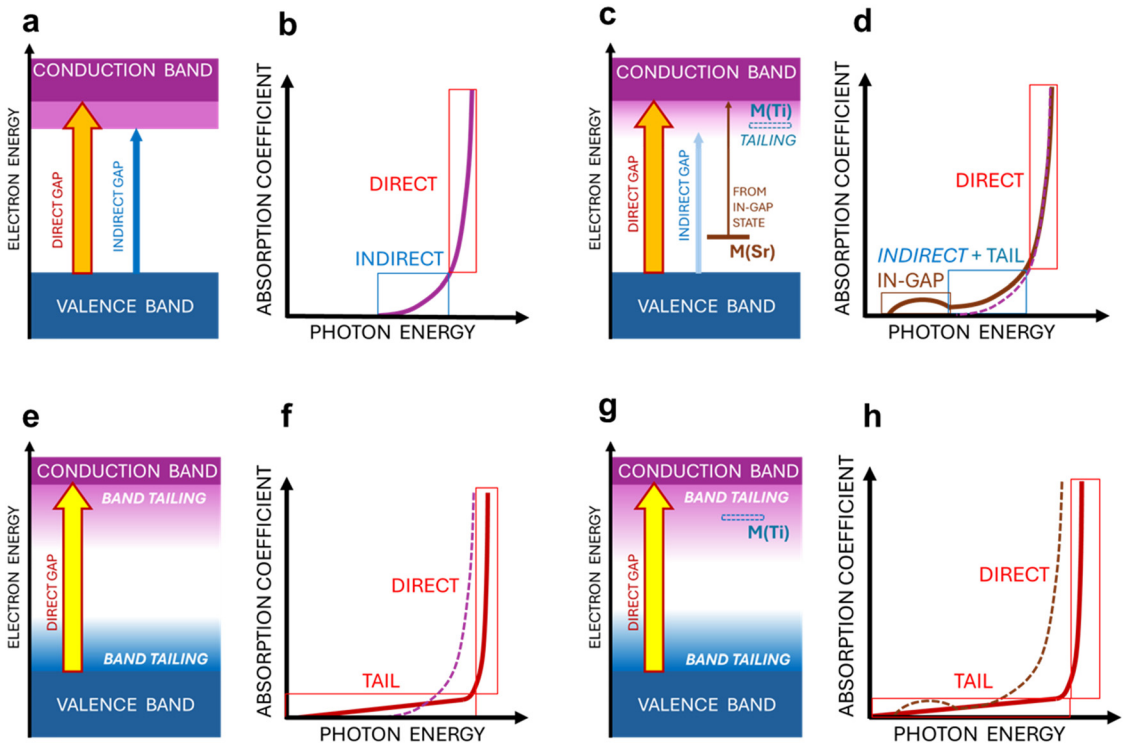

Fig. 7 Schematics of ((a), (c), (e) and (f)) band diagrams and ((b), (d), (f) and (h)) optical absorption in ((a) and (b)) unstressed STO, ((c) and (d)) unstressed MSTO, ((e) and (f)) strained STO film, and ((g) and (h)) strained MSTO film. Arrows show optical transitions in ((a), (c), (e) and (g)).

and fundamental absorption. Furthermore, because strain prohibits M(Sr) substitutions, there are no M(Sr)-related in-gap states and sub-gap absorption. Overall, the role of strain prevails over that of doping: the strained MSTO films are transparent in a broader spectral range than unstressed MSTO (Fig. 7h).

Thus, the experimentally studied optical absorption suggests that the M-substitution has no effect on the bandgaps and fundamental optical absorption in MSTO films. The substrate-imposed strain leads to the gap's widening and to the structural band's tailing. The M-dopants create the in-gap states contributing to the tails. First-principles analyses of the crystal and electronic band structures for the M-substitutions in thin films are highly desirable to support or discard the interpretations suggested here.

Conclusions

The effects of transition-metal (M = Mn, Fe, Co, Ni) substitution on the crystal structure, band structure, and optical absorption are studied in thin films of perovskite STO grown on LSAT, STO, Si, and SiO_2 substrates ensuring variations of lattice strain in the films. It is found that M-occupancy, fundamental optical absorption, bandgaps, and band tails are all regulated by substrate-induced strain. The M-dopants have no effect on bandgaps but produce in-gap states contributing to band tailing. The results imply that substrates can significantly modify the compositional effects in thin films.

Author contributions

M. T.: conceptualization; formal analysis; funding acquisition; supervision; writing – original draft; writing – review & editing. Writing – original draft. N. N.: investigation. O. P.: investigation. T. K.: investigation. V. V.: investigation. A. D.: funding acquisition.

Conflicts of interest

There are no conflicts to declare.

Data availability

The data supporting this article have been included as part of the SI. The supplementary information contains additional XRD and VASE data supporting this work. See DOI: **https://doi.org/10.1039/d5ma00732a**

Acknowledgements

The authors acknowledge support from the Czech Science Foundation (Grant No. 22-10832S) and the Czech Academy of Sciences through the program Strategy AV21 ''Breakthrough technologies for the future – sensing, digitization, artificial intelligence, and quantum technologies''. M. T. is grateful to L. L. Rusevich and E. A. Kotomin for sharing unpublished results and for valuable discussions.

References

1 M. E. Lines and A. M. Glass, *Principles and Applications of Ferroelectrics and Related Materials*, Clarendon Press, 2004.
2 Y. Xu, *Ferroelectric Materials and Their Applications*, Elsevier, 1991.
3 K. Uchino, *Ferroelectric Devices*, 2nd edn, CRC Press, Boca Raton, 2009.
4 X. K. Wei, N. Domingo, Y. Sun, N. Balke, R. E. Dunin-Borkowski and J. Mayer, *Adv. Energy Mater.*, 2022, **12**, 2201199.
5 Y. Wang, Z. Lv, L. Zhou, X. Chen, J. Chen, Y. Zhou, V. A. L. Roy and S. T. Han, *J. Mater. Chem. C*, 2018, **6**, 1600.
6 B. Sun, G. Zhou, L. Sun, H. Zhao, Y. Chen, F. Yang, Y. Zhao and Q. Song, *Nanoscale Horiz.*, 2021, **6**, 939.
7 K. Schnieders, C. Funck, F. Cüppers, S. Aussen, T. Kempen, A. Sarantopoulos, R. Dittmann, S. Menzel, V. Rana, S. Hoffmann-Eifert and S. Wiefels, *APL Mater.*, 2022, **10**, 101114.
8 P. Roy, S. Kunwar, D. Zhang, D. Chen, Z. Corey, B. X. Rutherford, H. Wang, J. L. MacManus-Driscoll, Q. Jia and A. Chen, *Adv. Electron. Mater.*, 2022, **8**, 2101392.
9 Y. Yang, B. Sun, G. Zhou, C. Ke, J. Zhang, Y. Zhou, S. Mao, J. Qin and Y. Zhao, *Mater. Today Commun.*, 2023, **35**, 105512.
10 M. A. Boda, R. L. Withers, Y. Liu, J. Ye and Z. Yi, *J. Mater. Chem. A*, 2022, **10**, 22977.
11 H. Wei, C. Yang, Y. Wu, B. Cao, M. Lorenz and M. Grundmann, *J. Mater. Chem. C*, 2020, **8**, 15575.
12 A. Kumar, A. Kumar and V. Krishnan, *ACS Catal.*, 2020, **10**, 10253.
13 F. T. Wagner and G. A. Somorjai, *Nature*, 1980, **285**, 559.
14 H. C. Chen, C. W. Huang, J. C. S. Wu and S. T. Lin, *J. Phys. Chem. C*, 2012, **116**, 7897.
15 E. García-López, G. Marcì, B. Megna, F. Parisi, L. Armelao, A. Trovarelli, M. Boaro and L. Palmisano, *J. Catal.*, 2015, **321**, 13.
16 S. Patial, V. Hasija, P. Raizada, P. Singh, A. A. P. K. Singh and A. M. Asiri, *J. Environ. Chem. Eng.*, 2020, **8**, 103791.
17 B. Moss, Q. Wang, K. T. Butler, R. Grau-Crespo, S. Selim, A. Regoutz, T. Hisatomi, R. Godin, D. J. Payne, A. Kafizas, K. Domen, L. Steier and J. R. Durrant, *Nat. Mater.*, 2021, **20**, 511.
18 Y. S. Hou, S. Ardo and R. Q. Wu, *Phys. Rev. Mater.*, 2021, **5**, 065801.
19 R. Joy and S. Haridas, *Int. J. Hydrogen Energy*, 2021, **46**, 1879.
20 Y. Yoshiyama, S. Hosokawa, H. Asakura, K. Teramura and T. Tanaka, *J. Phys. Chem. C*, 2022, **126**, 4415.
21 A. Viernstein, M. Kubicek, M. Morgenbesser, T. M. Huber, M. Siebenhofer and J. Fleig, *Mater. Adv.*, 2022, **3**, 2800.
22 C. Avcıoğlu, S. Avcıoğlu and M. F. Bekheet, *ACS Appl. Energy Mater.*, 2023, **6**, 1134.
23 C. Courter, J. Stewart and T. Cuk, *J. Phys. Chem. C*, 2023, **127**, 4905.
24 Z. L. Chen and M. H. Huang, *J. Mater. Chem. A*, 2023, **11**, 22198.
25 C. Wang, Y. Li, X. Cai, D. Duan and Q. Jia, *J. Mater. Chem. A*, 2023, **11**, 21046.

26 A. I. Lebedeva, I. A. Sluchinskaya, A. Erko and V. F. Kozlovskii, *JETP Lett.*, 2009, **89**, 457.
27 I. A. Sluchinskaya, A. I. Lebedeva and A. Erko, *Bull. Russ. Acad. Sci. Phys.*, 2010, **74**, 1235.
28 M. Valant, T. Kolodiazhnyi, I. Arcon, F. Aguesse, A. K. Axelsson and N. M. Alford, *Adv. Funct. Mater.*, 2012, **22**, 2114.
29 J. Kubacki, D. Kajewski, A. Koehl, M. Wojtyniak, R. Dittmann and J. Szade, *Radiat. Phys. Chem.*, 2013, **93**, 123.
30 R. A. Maier, E. Cockayne, M. Donohue, G. Cibin and I. Levin, *Chem. Mater.*, 2020, **32**, 4651.
31 G. M. Repa and L. A. Fredin, *Phys. Chem. Chem. Phys.*, 2021, **23**, 23486.
32 G. M. Repa and L. A. Fredin, *Appl. Phys. Lett.*, 2022, **121**, 022401.
33 R. A. Maier and C. A. Randall, *J. Am. Ceram. Soc.*, 2016, **99**, 3350.
34 R. B. Comes, T. C. Kaspar, S. M. Heald, M. E. Bowden and S. A. Chambers, *J. Phys.: Condens. Matter*, 2016, **28**, 035901.
35 A. Viernstein, M. Kubicek, M. Morgenbesser, G. Walch, G. C. Brunauer and J. Fleig, *Adv. Funct. Mater.*, 2019, **29**, 1900196.
36 N. H. Perry, N. Kim, E. Ertekin and H. L. Tuller, *Chem. Mater.*, 2019, **31**, 1030.
37 M. Morgenbesser, S. Taibl, M. Kubicek, A. Schmid, A. Viernstein, N. Bodenmuller, C. Herzig, F. Baiutti, J. de Dios Sirvent, M. O. Liedke, M. Butterling, A. Wagner, W. Artner, A. Limbeck, A. Tarancon and J. Fleig, *Nanoscale Adv.*, 2021, **3**, 6114.
38 J. Kubacki, D. Kajewski, J. Goraus, K. Szot, A. Koehl, Ch Lenser, R. Dittmann and J. Szade, *J. Chem. Phys.*, 2018, **148**, 154702.
39 I. A. Sluchinskaya and A. I. Lebedev, *Phys. Solid State*, 2022, **64**, 345.
40 R. A. Evarestov, S. Piskunov, E. A. Kotomin and G. Borstel, *Phys. Rev. B: Condens. Matter Mater. Phys.*, 2003, **67**, 064101.
41 R. Evarestov, E. Blokhin, D. Gryaznov, E. A. Kotomin, R. Merkle and J. Maier, *Phys. Rev. B: Condens. Matter Mater. Phys.*, 2012, **85**, 174303.
42 I. Suzuki, L. Gura and A. Klein, *Phys. Chem. Chem. Phys.*, 2019, **21**, 6238.
43 X. Lia, H. Zhao, N. Xu, X. Zhou, C. Zhang and N. Chen, *Int. J. Hydrogen Energy*, 2009, **34**, 6407.
44 S. Carlotto, M. M. Natile, A. Glisenti, J. F. Paul, D. Blanc and A. Vittadini, *Phys. Chem. Chem. Phys.*, 2016, **18**, 33282.
45 F. Ichihara, Y. Murata, H. Ono, C. K. Choo and K. Tanaka, *Appl. Surf. Sci.*, 2017, **419**, 126.
46 Y. Liua, S. Baumann, F. Schulze-Küppers, D. N. Mueller and O. Guillon, *J. Eur. Ceram. Soc.*, 2018, **38**, 5058.
47 Y. Yoshiyama, S. Hosokawa, H. Asakura, K. Teramura and T. Tanaka, *J. Phys. Chem. C*, 2022, **126**, 4415.
48 F. B. L. B. Siqueira and D. C. Campos, *Solid State Ionics*, 2023, **391**, 116140.
49 I. A. Sluchinskaya and A. I. Lebedev, *Phys. Solid State*, 2019, **61**, 390.
50 I. A. Sluchinskaya and A. I. Lebedev, *J. Alloys Compd.*, 2020, **820**, 153243.
51 A. Mizera and E. Drożdż, *Ceram. Int.*, 2020, **46**, 24635.
52 F. Alarab, K. Hricovini, B. Leikert, L. Nicolaï, M. Fanciulli, O. Heckmann, C. Richter, L. Prušakova, Z. Jansa, P. Šutta, J. Rault, P. Lefevre, M. Sing, M. Muntwiler, R. Claessen and J. Minár, *Phys. Rev. B*, 2021, **104**, 165129.
53 I. A. Sluchinskaya, A. I. Lebedev and A. Erko, *J. Adv. Dielectr.*, 2013, **3**, 1350031.
54 A. I. Lebedev and I. A. Sluchinskaya, *Ferroelectrics*, 2016, **501**, 1.
55 R. A. Maier, A. C. Johnston-Peck and M. P. Donohue, *Adv. Funct. Mater.*, 2016, **26**, 8325.
56 *Epitaxial Growth of Complex Metal Oxides*, ed. G. Koster, M. Huijben, G. Rijnders, Woodhead Publishing, 2022.
57 N. A. Pertsev, A. G. Zembilgotov and A. K. Tagantsev, *Phys. Rev. Lett.*, 1998, **80**, 1988.
58 N. A. Pertsev, A. K. Tagantsev and N. Setter, *Phys. Rev. B: Condens. Matter Mater. Phys.*, 2000, **61**, R825.
59 J. H. Haeni, P. Irvin, W. Chang, R. Uecker, P. Reiche, Y. L. Li, S. Choudhury, W. Tian, M. E. Hawley, B. Craigo, A. K. Tagantsev, X. Q. Pan, S. K. Streiffer, L. Q. Chen, S. W. Kirchoefer, J. Levy and D. G. Schlom, *Nature*, 2004, **430**, 758.
60 K. J. Choi, M. Biegalski, Y. L. Li, A. Sharan, J. Schubert, R. Uecker, P. Reiche, Y. B. Chen, X. Q. Pan, V. Gopalan, L.-Q. Chen, D. G. Schlom and C. B. Eom, *Science*, 2004, **306**, 1005.
61 D. G. Schlom, L.-Q. Chen, C. J. Fennie, V. Gopalan, D. A. Muller, X. Pan, R. Ramesh and R. Uecker, *MRS Bull.*, 2014, **39**, 118.
62 R. F. Berger, C. J. Fennie and J. B. Neaton, *Phys. Rev. Lett.*, 2011, **107**, 146804.
63 M. Tyunina, N. Nepomniashchaia, V. Vetokhina and A. Dejneka, *Appl. Phys. Lett.*, 2020, **117**, 082901.
64 M. Tyunina, L. L. Rusevich, E. A. Kotomin, O. Pacherova, T. Kocourek and A. Dejneka, *J. Mater. Chem. C*, 2021, **9**, 1693.
65 M. Tyunina, N. Nepomniashchaia, V. Vetokhina and A. Dejneka, *APL Mater.*, 2021, **9**, 121108.
66 M. Tyunina, M. Savinov, O. Pacherova, T. Kocourek, P. Yudin and A. Dejneka, *APL Mater.*, 2025, **13**, 031101.
67 N. Nepomniashchaia, O. Pacherova, T. Kocourek, A. Dejneka and M. Tyunina, *J. Appl. Phys.*, 2025, **137**, 014103.
68 T. Yamada, B. Wylie-van Eerd, O. Sakata, A. K. Tagantsev, H. Morioka, Y. Ehara, S. Yasui, H. Funakubo, T. Nagasaki and H. J. Trodahl, *Phys. Rev. B*, 2015, **91**, 214101.
69 M. Tyunina, J. Levoska, O. Pacherova, T. Kocourek and A. Dejneka, *J. Mater. Chem. C*, 2022, **10**, 6770.
70 D. A. Freedman, D. Roundy and T. A. Arias, *Phys. Rev. B: Condens. Matter Mater. Phys.*, 2009, **80**, 064108.
71 E. Clouet, C. Varvenne and T. Jourdan, *Comput. Mater. Sci.*, 2018, **147**, 49.
72 R. J. Elliott, *Phys. Rev.*, 1957, **108**, 1384.
73 J. Tauc, R. Grigorovic and A. Vancu, *Phys. Status Solidi B*, 1966, **15**, 627.
74 M. Fox, *Optical Properties of Solids*, Oxford University Press, 2001.

75 M. Grundmann, Semiconductor Physics, *An Introduction Including Device and Nanophysics*, Springer, 2005.
76 B. D. Viezbicke, S. Patel, B. E. Davis and D. P. Birnie, *Phys. Status Solidi B*, 2015, **252**, 1700.
77 J. Klein, L. Kampermann, B. Mockenhaupt, M. Behrens, J. Strunk and G. Bacher, *Adv. Funct. Mater.*, 2023, **33**, 2304523.
78 M. L. Cohen and J. R. Chelikowsky, *Electronic Structure and Optical Properties of Semiconductors*, Springer, 1989.
79 P. Yu and M. Cardona, *Fundamentals of Semiconductors*, Springer, 1996.
80 M. Tyunina, L. D.Yao, D. Chvostova, T. Kocourek, M. Jelinek, A. Dejneka and S. van Dijken, *New J. Phys.*, 2015, **17**, 043048.
81 F. Urbach, *Phys. Rev.*, 1953, **92**, 1324.
82 H. W. Martienssen, *J. Phys. Chem. Solids*, 1957, **2**, 257.
83 M. V. Kurik, *Phys. Stat. Sol. (a)*, 1971, **8**, 9.
84 J. D. Dow and D. Redfield, *Phys. Rev. B: Condens. Matter Mater. Phys.*, 1972, **5**, 594.
85 C. M. Soukoulis, M. H. Cohen and E. N. Economou, *Phys. Rev. Lett.*, 1984, **53**, 616.
86 S. John, C. Soukoulis, M. H. Cohen and E. N. Economou, *Phys. Rev. Lett.*, 1986, **57**, 1777.
87 G. D. Cody, *J. NonCryst. Solids*, 1992, **141**, 3.
88 P. Van Mieghem, *Rev. Mod. Phys.*, 1992, **64**, 755.
89 I. Studenyak, Ml Kranjčec and M. Kurik, *Int. J. Opt. Appl.*, 2014, **4**, 76.